THE JOURNAL OF PHYSICAL CHEMISTRY C

Article

pubs.acs.org/JPCC

Interaction of Titanium Oxide Nanostructures with Graphene and Functionalized Graphene Nanoribbons: A DFT Study

Serge Ayissi,[†] Paul A. Charpentier,*[,†] Nasrin Farhangi,[†] Jeffery A. Wood,[†] Krisztián Palotás,[‡] and Werner A. Hofer[§]

[†]Department of Chemical and Biochemical Engineering, University of Western Ontario, London, Ontario N6A 5B9, Canada

[‡]Department of Theoretical Physics, Budapest University of Technology and Economics, Budapest, Hungary

[§]Surface Science Research Centre, University of Liverpool, Liverpool L69 3BX, United Kingdom

Supporting Information

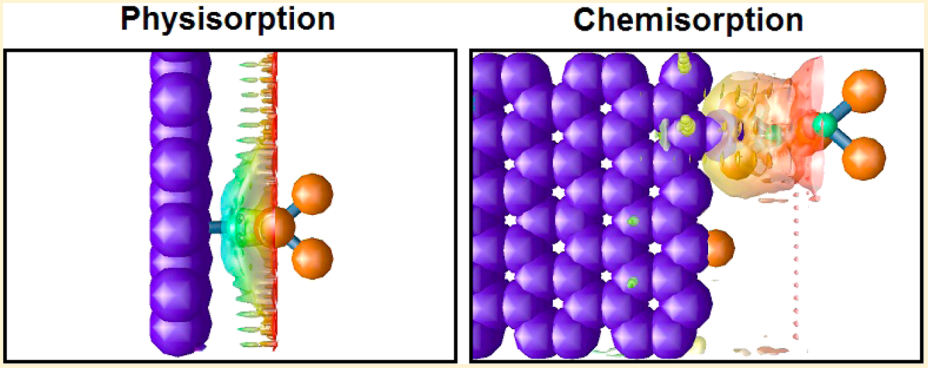

ABSTRACT: Graphene substrates are known to have randomly located functional groups on their surface, particularly at their edges, including carboxylate, carbonyl, epoxy, and alcohol functionalities. However, the detailed interactions of these graphene functionalities with metal oxide nanoclusters are unexplored. This work examined the interaction of titania nanostructures with both graphene and functionalized graphene nanoribbons (GNRs) using density functional theory (DFT) calculations. The interactions of TiO_2 (anatase, rutile, and molecular) with graphene were found to favor the physisorption of rutile titania. The interactions of TiO_2 with GNRs were found to considerably improve the strength of the nanostructure binding to the substrate with rutile and anatase showing similar chemisorption. Charge density maps showed the importance of the electron distribution in the interaction between titania and graphene with chemisorption sites. Valuable information on the strength of the binding energies was determined by studying the electronic structure using partial density of states (PDOS) of the TiO_2/graphene systems at specific adsorption sites. These results show the potential for controlled and oriented growth mechanisms that have applications in next generation photovoltaic and photocatalytic devices.

1. INTRODUCTION

Graphene has attracted considerable attention for a diverse range of applications, including composites,[1] electronics,[2] sensors,[3] optical, and energy applications.[4] Graphene, a two-dimensional (2-D) form of carbon is composed of a single layer of atoms arranged in a honeycomb lattice that can possess theoretical surface areas of up to ~2 600 m^2/g.[5] This 2-D nanostructure has attracted significant attention even when compared to carbon nanotubes (CNTs), as its high surface area approaches the theoretical maximum for a single-walled carbon nanotube (SWCNT) and is considerably higher than bundles of nanotubes or multiwalled CNTs.[6] Graphene has very high thermal and electrical conductivity[7] which is desirable for improving the physical and mechanical properties of composites. Also of interest are finite-width, single-layer graphene stripes known as graphene nanoribbons (GNRs).[8−11] These materials are similar to SWCNTs, possessing either metallic or semiconducting properties based on the orientation of the crystallographic axis.[12] Functionalized graphene nanoribbons (FGNRs) have been the subject of extensive experimental and theoretical research because of the presence of edges (finite graphene) which make their electronic properties unique.

Titanium dioxide (TiO_2) is a well-known semiconductor material investigated for a variety of applications, including environmental remediation[13] and photovoltaic materials such as dye-sensitized solar cells (DSSCs).[14,15] The two main crystalline structures of TiO_2 are anatase and rutile.[16] Anatase belongs to the space group $I4_1/amd$ (D_{4h}^{19}), containing 12 atoms per primitive cell as Ti_4O_8. Rutile structure belongs to the space group $P4_2/mnm$ (D_{4h}^{19}) containing 6 atoms per primitive cell as Ti_2O_4. Rutile is a thermodynamically stable phase possessing a

Received: April 17, 2013
Revised: October 19, 2013

   dx.doi.org/10.1021/jp403835m | J. Phys. Chem. C XXXX, XXX, XXX−XXX

band gap energy[17] (3.0 eV) smaller than that of anatase[18] (3.2 eV) although exhibiting less photactivity and a higher electron−hole recombination rate.[16]

A large amount of research has aimed to modify the properties of TiO_2, specifically to decrease the electron−hole recombination rate while extending its light absorption into the visible region.[13] Graphene has a large electron-storage capacity and its carbon atoms are considered good electron acceptors. These atoms serve as charge-trapping sites, reducing the electron−hole recombination rate to enhance the photocatalytic activity of titania.[19,20] Graphene can also act as a photosensitizer to enhance the optical response in the visible light region.[21] Previously, we examined the synthesis of titania−graphene composites and iron-doped titania nanoassemblies in supercritical CO_2,[22] as well as their resulting properties,[23] which improved because of metal oxide alignment, although the origins of the alignment were unexplained. Our group has also carried out DFT simulations on the behavior of titania in CO_2, demonstrating CO_2-philic properties arising from the metal acetate group,[24,25] illustrating the importance of theoretical calculations for understanding the physical and chemical mechanisms operating in these systems.

Presently, only a few theoretical studies exist for investigating the interaction between TiO_2 nanostructures and graphene. Rojas et al. used DFT calculations[26] for titanium-modified graphene for the adsorption of different molecules, showing that this approach could explain the higher hydrogen storage capacity of a hybrid system compared to that of plain graphene. They also showed that nitrogen and water molecules could be adsorbed, albeit with lower selectivity than hydrogen molecules. Despite the great interest in titania−graphene composites, the details on the chemical and electronic interactions between nanostructural TiO_2 and graphene or functionalized GNRs have not been investigated theoretically. In the present study, we investigate the interactions of TiO_2 and graphene or GNRs through two possible adsorption mechanisms: physisorption and chemisorption.

2. COMPUTATIONAL DETAILS

Electronic structure calculations were carried out using the GGA PW91[27] implemented in VASP code[28,29] for all graphene, graphene nanoribbons (GNRs), and titania systems. The electron−ion interactions were described by a projector-augmented wave (PAW) scheme.[30,31] The electronic wave functions were expanded using plane waves up to a kinetic energy of 400 eV with the k-point sampling set to $3 \times 2 \times 1$ for the geometry optimization and to $5 \times 5 \times 1$ for the electronic structure. The spin-polarization approach was implemented in all calculations. The Brillouin zone was described using a Monkhorst−Pack[32] (M&P) scheme of special k-points to obtain a convergence criteria of 5.10×10^{-3} eV for energies and 0.01 eV/Å for structural variations between two different k-point grids. Band diagrams and partial density of states (PDOS) analysis were obtained by fixing the Wigner−Seitz radius (rwigs) for the support during integration over the number of electrons and then by setting rwigs for the adsorbates within the radii of tangential spheres. This method allowed the accurate assignment of relevant atomic orbital attributions to a particular projected DOS peak. All systems were modeled using the supercell approach with periodically repeated slabs. Models of a clean graphene sheet and two functionalized graphene nanoribbons were used. Six adsorption sites were considered: top, bridge, hollow sites on the pure graphene sheet, and graphene-ol, carboxylate and epoxy sites on the functionalized GNRs. Figure 1a−c shows the schematic structures of titania species adsorbed on all possible sites of a pure graphene sheet while Figure 1d−f shows the possible adsorption sites for titania species on FGNRs.

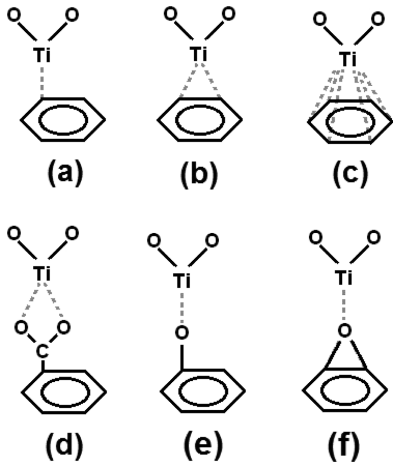

Figure 1. Adsorption sites of clean graphene and functionalized graphene nanoribbons. TiO_2 adsorbates can possibly be located at (a) top, (b) bridge, and (c) hollow sites of graphene. TiO_2 can also be located at (d) carboxylate, (e) graphene-ol, and (f) epoxy sites of functionalized graphene nanoribbons (GNRs).

A typical graphene supercell (lozenge shaped) can be set up using the two primitive vectors $\mathbf{a}_1$ and $\mathbf{a}_2$, and the lattice parameter of the graphene honeycomb structure $\mathbf{a}_0$. The primitive vectors of graphene are

$$\mathbf{a}_1 = \frac{a_0}{2}(3, \sqrt{3}, 0), \quad \mathbf{a}_2 = \frac{a_0}{2}(3, -\sqrt{3}, 0)$$

where a_0 = 1.42 Å is the C−C bond length. With these vectors and the primitive cell, a $2 \times 5a_1 \times 5a_2$ = 50 atoms supercell can be constructed, as shown in Figure 2a.

To accurately study the physical and chemical adsorption of larger structures, square graphene sheet systems need to be constructed. A four-atom unit cell and two perpendicular lattice vectors were chosen to construct a square lattice. The 2 new vectors are

$$\mathbf{a}_3 = a_0(3, 0, 0), \quad \mathbf{a}_4 = a_0(0, \sqrt{3}, 0)$$

With these new vectors and the four-atom unit cell, a $4 \times 5a_3 \times 5a_4$ = 100 atom supercell was constructed as shown in Figure 2b.

Functionalization of graphene occurs preferentially at the edges.[33] As the limitations of DFT calculations allow only small system sizes, functionalized graphene nanoribbons were used as a replacement for functionalized graphene sheets. The supercell used for the chemical adsorption study was initially a $4 \times 3a_3 \times 5a_4$ = 60 carbon atoms cell. This graphene supercell was then functionalized on its armchair side and as a result becomes what is termed an armchair graphene nanoribbon (A-GNR). Functionalization on the zigzag side of the same initial supercell created a zigzag graphene nanoribbon (Z-GNR). Functionalization on the edges of the GNRs was made by hydrogen atoms, an alcohol group (OH), or a carboxylate group (COO−), while functionalization on the GNR surface was examined using an epoxy group (−O−). Figures 3a and 3b show the 10 × 3 A-

dx.doi.org/10.1021/jp403835m | J. Phys. Chem. C XXXX, XXX, XXX−XXX

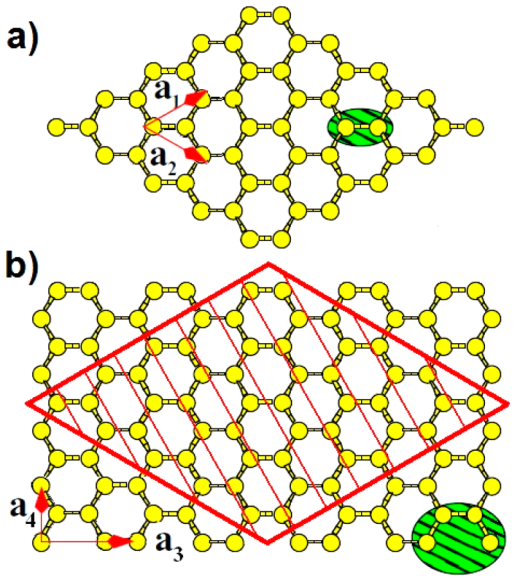

Figure 2. Graphene supercells. (a) The supercell of primitive parameters has $2 \times 5a_1 \times 5a_2 = 50$ atoms with a two-atom unit cell. (b) The reconstructed supercell has $4 \times 5a_3 \times 5a_4 = 100$ atoms with a four-atom unit cell.

GNR and 6 × 5 Z-GNR, respectively, used for the chemical adsorption study of titania on GNRs.

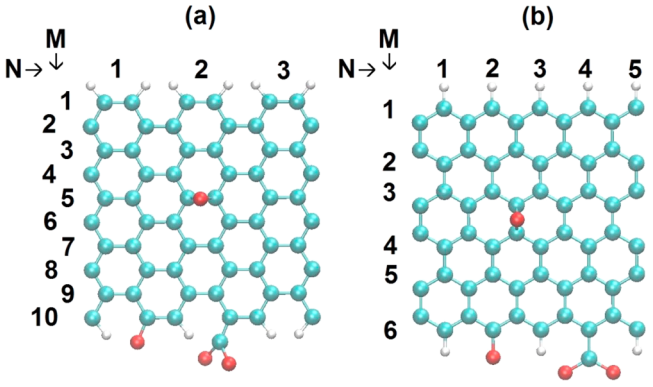

Figure 3. Scheme of (H), (O), and (COO) terminated (a) 10 × 3 armchair graphene nanoribbon (A-GNR) and (b) 6 × 5 zigzag graphene nanoribbon (Z-GNR). Periodic boundary conditions are assumed in the *x* direction. *M* and *N* are the numbers of columns and rows, respectively, of atoms used to label the $M \times N$ ribbon.

Functionalized A-GNR is periodic and infinite on its zigzag side and finite on its functionalized armchair side. Functionalized Z-GNR is periodic and infinite on its armchair side and finite on its functionalized zigzag side. Figure 4a shows the pure graphene supercell simulation box utilized in the DFT calculations. This graphene sheet is 2-dimensionally periodic and is separated from its own periodic image by a vacuum of 25 Å on the *z* axis. Figures 4b and 4c show respectively armchair and zigzag GNRs delimited by the size of their simulation boxes. These two GNR sheets are 1-dimensionally periodic and are separated from their own periodic image by a vacuum of 20 Å on the *z* axis. The functionalized edges of the GNRs are separated by 10 Å of vacuum on the *y* axis from their own images.

Models of a TiO_2 molecule, the smallest stoichiometric rutile nanostructure (Ti_2O_4), and the smallest stoichiometric anatase nanostructure (Ti_4O_8) were used. The TiO_2 molecule was converged in vacuum for its noncrystalline properties, whereas rutile (Ti_2O_4) and anatase (Ti_4O_8) were converged in the bulk. While in vacuum, rigid structures were set up for both rutile and anatase because of the already reported metastability of small sized titania nanostructures of bulk properties.[34,35] Figure 5 shows the schematic structures of the titania species adsorbed on graphene.

The isolated TiO_2 molecule was calculated in a large rectangular supercell ($10.0 \times 10.0 \times 20.0$ Å^3) and structurally optimized. The rutile TiO_2 unit cell (Ti_2O_4) was initially calculated in a small rectangular supercell ($4.6 \times 4.6 \times 2.9$ Å^3) for a structural optimization of bulk properties. Then the isolated rutile had its wave function optimized in a large rectangular supercell ($10.0 \times 10.0 \times 20.0$ Å^3). The anatase TiO_2 unit cell (Ti_4O_8) was initially calculated in a small rectangular supercell ($3.7 \times 3.7 \times 9.5$ Å^3), to provide geometry optimization in the bulk. Anatase had its wave function optimized in a large rectangular supercell ($10.0 \times 10.0 \times 20.0$ Å^3). Spin polarization was considered in all calculations, and the electronic structures were optimized to their ground state. Ti–O nanostructure optimized bond distances and angles that were used in the DFT calculations are shown in Table 1. The structure of the anatase unit cell is more compact than that of rutile as the bond distances and angles are slightly smaller.[16,36–38] The TiO_2 molecule was optimized in vacuum as previously stated and as a result has no nonbonded interactions.

Adsorption Energy Determination. The adsorption energy values, bond lengths, and angles are listed in Table 2. The adsorption energy (E_{ads}) is calculated according to the formula

$$E_{ads} = E_{(TiO_2/graphene)} - (E_{TiO_2} + E_{graphene})$$

where $E_{graphene}$, E_{TiO_2}, and $E_{TiO_2/graphene}$ denote the calculated energy of a clean graphene sheet, isolated titanium oxide molecule or nanostructure in vacuum, and the total energy of a TiO_2/graphene unit cell adsorbed to the graphene sheet, respectively. A negative value of E_{ads} implies that the adsorption of the crystalline TiO_2 adsorbate is thermodynamically stable on its graphene substrate.

3. RESULTS AND DISCUSSION

Physical Adsorption of Titania Species on Graphene. Graphene has three main physical adsorption sites: top, bridge, and hollow sites as described in Figure 1. The results of DFT-calculated nonbonded Ti–C binding energies and distances between titania and graphene are shown in Table 2. These adsorption sites depend on the geometry of the adsorbate and the direction of adsorption. Rotating the adsorbate by 90° created the "rotated" version of a physical adsorption site.

Figure 6a provides a comparison of the adsorption strength of the three studied species, i.e., molecular TiO_2, rutile (Ti_2O_4), and anatase (Ti_4O_8) adsorbed at similar adsorption sites that are the top, bridging, and the hollow site of pure graphene. Figure 6b shows these adsorption sites of graphene with the titania adsorbates rotated by 90°.

As shown in Table 2, molecular TiO_2 was found to adsorb preferentially on a bridge site of pure graphene[26] (i.e., lowest E_{ads}), followed by the hollow site and then the top site. Of the rotated structures, the rotated hollow site was found to be the

dx.doi.org/10.1021/jp403835m | J. Phys. Chem. C XXXX, XXX, XXX–XXX

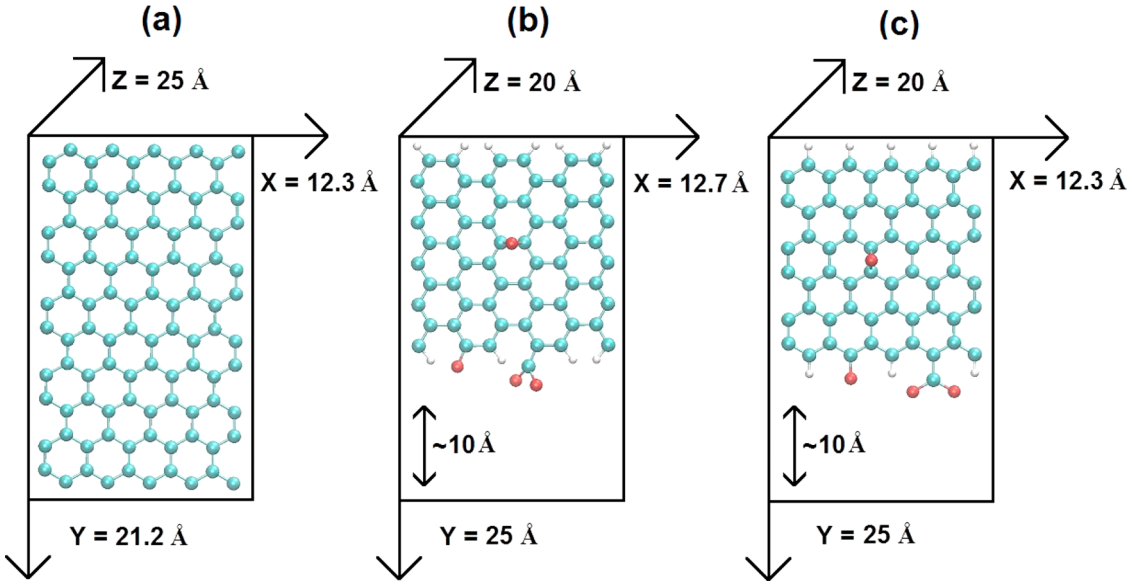

Figure 4. Supercells and box sizes of (a) graphene, (b) armchair-GNR, and (c) zigzag-GNR.

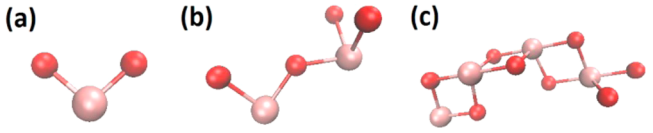

Figure 5. Optimized structures of (a) an isolated TiO_2 molecule, (b) an isolated rutile unit cell (Ti_2O_4), and (c) an isolated anatase unit cell (Ti_4O_8).

Table 1. GGA-PW91[27] Ground States Bond Angles and Distances in the Vacuum for Molecular TiO_2 and in the Bulk for Structural Rutile (Ti_2O_4) and Anatase (Ti_4O_8)

parameters	TiO_2 vacuum	Ti_2O_4 (rutile) bulk properties	Ti_4O_8 (anatase) bulk properties
d_{Ti-O} (b.)	1.67 Å	1.96 Å	1.83 Å
d_{Ti-Ti} (n.b.)	–	3.61 Å	3.03 Å
d_{O-O} (n.b.)	–	2.57 Å	2.29 Å
O–Ti–O	110.6°	81.6°	74.1°
Ti–O–Ti	–	130.8°	105.9°

Table 2. Adsorption Energies and Nonbonded Ti–C Distances for TiO_2 Species Adsorbed on Pure Graphene Sheets

	molecular TiO_2		rutile or Ti_2O_4		anatase or Ti_4O_8	
adsorption sites	E_{ads} (eV)	Ti–C (Å)	E_{ads} (eV)	Ti–C (Å)	E_{ads} (eV)	Ti–C (Å)
top	−1.11	2.56	−1.93	2.28	−1.42	2.19
bridge	−1.21	2.60	−2.02	2.33	−1.43	2.30
hollow	−1.18	2.78	−2.25	2.50	−1.95	2.45
rotated top	−1.17	2.56	−1.94	2.27	−1.36	2.22
rotated bridge	−1.11	2.64	−1.83	2.39	−1.13	2.35
rotated hollow	−1.22	2.78	−2.21	2.54	−1.87	2.42

most favorable adsorption followed by the rotated top and then the rotated bridge. These binding energy values correspond to Ti–C nonbonded interactions for the physical adsorption process. Rutile (Ti_2O_4) was found to adsorb preferentially on a hollow site, followed by the bridge site and then the top site of pure graphene. For rutile, similar to what was found for molecular TiO_2, the rotated hollow site was found to be the most favorable of the rotated graphene structures. Similar to rutile, anatase (Ti_4O_8) was found to adsorb preferentially on a hollow site, followed by the bridge site and then the top site of pure graphene. Of the rotated structures, anatase was most favorable on the rotated hollow site.

Chemical Adsorption of Titania Species on Graphene Nanoribbons. Functionalized graphene nanoribbons (FGNRs) have additional adsorption sites, epoxy, graphene-ol, and carboxylate, that can be introduced onto their surface during synthesis, which are concentrated at the nanoribbon edge.[23] Functionalized armchair graphene nanoribbon (A-GNR) and the zigzag graphene nanoribbon (Z-GNR) were used to calculate all the chemical adsorption energies and distances using the three titania adsorbates on the sites, termed graphene-ol, carboxylate, and epoxy. The results of these DFT-calculated, nonbonded Ti–O binding energies and distances between titania and functionalized GNRs are shown in Table 3.

As shown in Table 3, molecular TiO_2 was found to adsorb preferentially on the carboxylate site followed by the graphene-ol site and then on the epoxy adsorption site of the functionalized A-GNR. The TiO_2 molecule was found to have a similar pattern on Z-GNR compared with that of A-GNR. Molecular TiO_2 adsorbed at the carboxylate sites of functionalized A-GNR and Z-GNR shows higher adsorption interactions of E_{ads} = −3.27 eV and at a d_{Ti-O} = 2.09 Å and E_{ads} = −3.38 eV and at a d_{Ti-O} = 2.11 Å, respectively, corresponding to a Ti–O nonbonded interaction in the chemical adsorption phenomenon. The epoxy adsorption site of the GNRs was found to have the weakest binding energy of the investigated Ti–O nonbonded interactions. Similar to molecular TiO_2, Rutile (Ti_2O_4) was found to adsorb preferentially on the edge-located carboxylate site, followed by the edge-located graphene-ol site, and then on the surface-located epoxy adsorption site of A-GNR. Rutile (Ti_2O_4) was also found to have a similar chemical adsorption pattern on both Z-GNR and A-GNR. Similar to rutile, Anatase (Ti_4O_8) was found to adsorb

dx.doi.org/10.1021/jp403835m | J. Phys. Chem. C XXXX, XXX, XXX–XXX

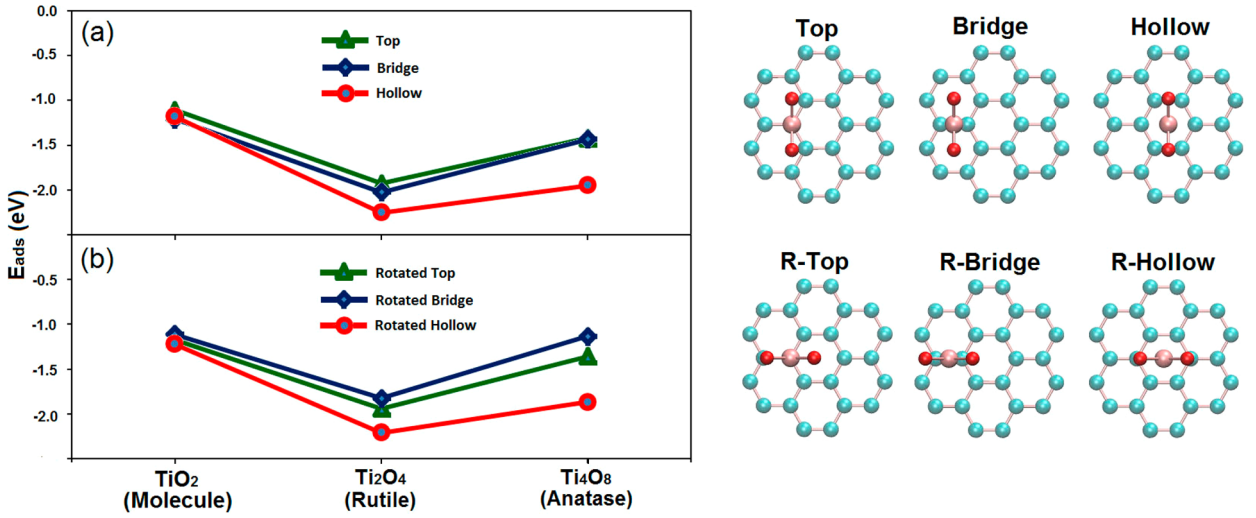

Figure 6. Adsorption energies of TiO_2 adsorbates on functionalized graphene sheets. (a) Adsorption energy per titania species adsorbed on graphene at the normal physical adsorption sites: top, bridge, and hollow. (b) Adsorption energy per titania species adsorbed on graphene at the rotated physical adsorption sites: rotated top (R-Top), rotated bridge (R-Bridge), and rotated hollow (R-Hollow).

Table 3. Adsorption Energies and Nonbonded Ti−O Distances for TiO_2 Species Adsorbed on Functionalized Armchair and Zigzag Graphene Nanoribbons (GNRs)

	molecular TiO_2		rutile or Ti_2O_4		anatase or Ti_4O_8	
adsorption sites	E_{ads} (eV)	Ti−O (Å)	E_{ads} (eV)	Ti−O (Å)	E_{ads} (eV)	Ti−O (Å)
epoxy (arm)	−1.86	2.26	−2.97	2.17	−2.25	2.14
epoxy (zig)	−1.89	2.25	−3.02	2.16	−2.27	2.15
carboxylate (arm)	−3.27	2.09	−5.42	2.01	−5.33	1.95
carboxylate (zig)	−3.38	2.11	−5.48	2.01	−5.39	1.92
graphene-ol (arm)	−2.05	2.00	−3.23	1.91	−2.50	1.89
graphene-ol (zig)	−2.02	2.02	−3.15	1.92	−2.52	1.89

preferentially on the edge-located carboxylate site, followed by the edge-located graphene-ol site, and then on the surface-located epoxy adsorption site of the functionalized A-GNR. Once again, anatase (Ti_4O_8) was found to have a similar pattern on Z-GNR compared to that on A-GNR.

Figure 7a provides a comparison of the adsorption values of molecular TiO_2, rutile (Ti_2O_4), and anatase (Ti_4O_8) adsorbed at the chemical adsorption sites of the functionalized A-GNR that are the graphene-ol, carboxylate, and the epoxy sites. Figure 7b shows an identical comparison of the adsorption strength of the titania species on the chemical adsorption sites of the Z-GNR.

In order to understand the difference between molecular TiO_2, rutile (Ti_2O_4), and anatase (Ti_4O_8), binding energies and distances were compared on all adsorption sites. Molecular TiO_2 physisorbs on graphene with a lower energy and at a longer Ti−C distance. The same pattern can be observed with molecular TiO_2 binding to A-GNR and Z-GNR compared to nanostructural TiO_2 species. A TiO_2 molecule chemisorbs on GNRs with a binding energy (from 2 to 3 eV) lower than that of structural TiO_2 and at a longer distance of adsorption. For all TiO_2 species, the carboxylate adsorption sites are the most favorable. The epoxy sites are the most favorable on-surface

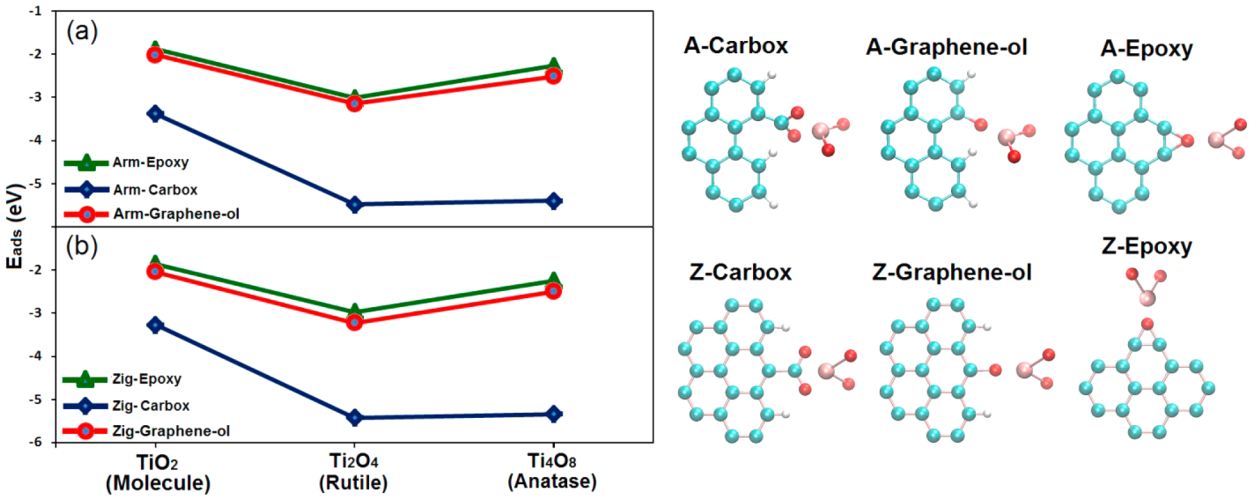

Figure 7. Adsorption energies of TiO_2 species on functionalized graphene nanoribbons. (a) Titania species adsorbed on armchair-graphene nanoribbons, (b) Titania species adsorbed on zigzag-graphene nanoribbons.

dx.doi.org/10.1021/jp403835m | J. Phys. Chem. C XXXX, XXX, XXX−XXX

adsorption sites. Previous theoretical simulations have shown that the organic groups on functionalized GNRs play a key role for nucleation sites for metal oxides.[39] The calculated strength of binding energy on functionalized GNRs sites confirms this tendency. Structural TiO_2 adsorbates show much stronger binding energies (from 2.5 to 5.5 eV) and distances than molecular TiO_2. Anatase (Ti_4O_8) generally adsorbs at a closer Ti−O and Ti−C distance from graphene and functionalized GNRs than rutile (Ti_2O_4), but with lower binding energies. In explanation, it has been recently shown that the lower binding strength of gas-phase titania compared to both rutile and anatase crystalline phase is due to a higher entropy as gas-phase TiO_2 is considered a 3D gas and nanostructural TiO_2 species are considered confined lattices.[40]

Electronic Structure of TiO_2−Graphene Interactions. Additional understanding on the difference of adsorption energy for TiO_2 species adsorbed on physical adsorption sites compared to the same species adsorbed on chemical adsorption sites can be gained by calculating the real space charge redistribution upon adsorption of titania on graphene substrates. The strength of the binding energy may have electrostatic origins. Figure 8a shows the electrostatic density

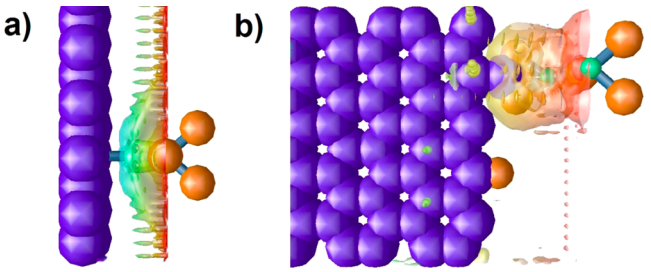

Figure 8. GGA-PW91 real space view of the charge distribution for (a) Ti_2O_4 physisorbed on top site of pure graphene and (b) Ti_2O_4 chemisorbed on carboxylate site of Z-GNR.

map at the binding energy region of Ti_2O_4 adsorbed on a top site of pure graphene. Figure 8b shows the corresponding electrostatic density map at the binding energy region of Ti_2O_4 adsorbed at a carboxylate site of functionalized Z-GNR. Both nonbonded interaction density maps indicate that the original electronic densities along the z direction of the adsorption region. The Ti−C interaction of Ti_2O_4 with a top site of graphene is perpendicular to the graphene surface and the electrostatic Ti−O interaction of Ti_2O_4 with carboxylate of Z-GNR is parallel to the GNR surface and located on its edge.

The density map in Figure 8a shows no clear electrostatic interaction between carbon atoms of the graphene substrate and titania as a clear electron gap separates graphene to rutile TiO_2 along the z axis. Most of the rutile electronic density is mainly due to the presence of oxygen. The density map shows a minimum force of attraction between titania and graphene due to electrostatic forces. The density contour of Figure 8b shows a much larger electrostatic interaction between COO− of Z-GNR and titania. A clear concentration of charge renders a continuous electron density along the z axis. The electrostatic density of the titania−COO binding region confirms the presence of a maximum force of attraction essentially due to an ionic carboxylate adsorption site. The charge of carboxylate is increasingly accumulated along the nonbonded interaction axis of the TiO_2−GNR binding region. These maps confirm the importance of the electron distribution property in the interaction between titania and graphene.

Although the electronic structure of rutile and anatase TiO_2 were previously investigated,[11,42] along with clean graphene,[41,42] the electronic structure of TiO_2 on graphene has not yet been considered. Hence, we investigated the partial density of states (PDOS) of TiO_2 nanostructures adsorbed on graphene at the calculated most stable adsorption site, i.e., the hollow site. After the binding energetics and structural morphologies of TiO_2 clusters adsorbed on graphene and functionalized graphene sheets were investigated, the electronic structures of all systems were studied in order to determine the relation between PDOS and the adsorption type of structural TiO_2 on graphene. The PDOS for O 2p and Ti 3d bands of anatase (Ti_4O_8) and rutile (Ti_2O_4) are displayed in Figures 9a

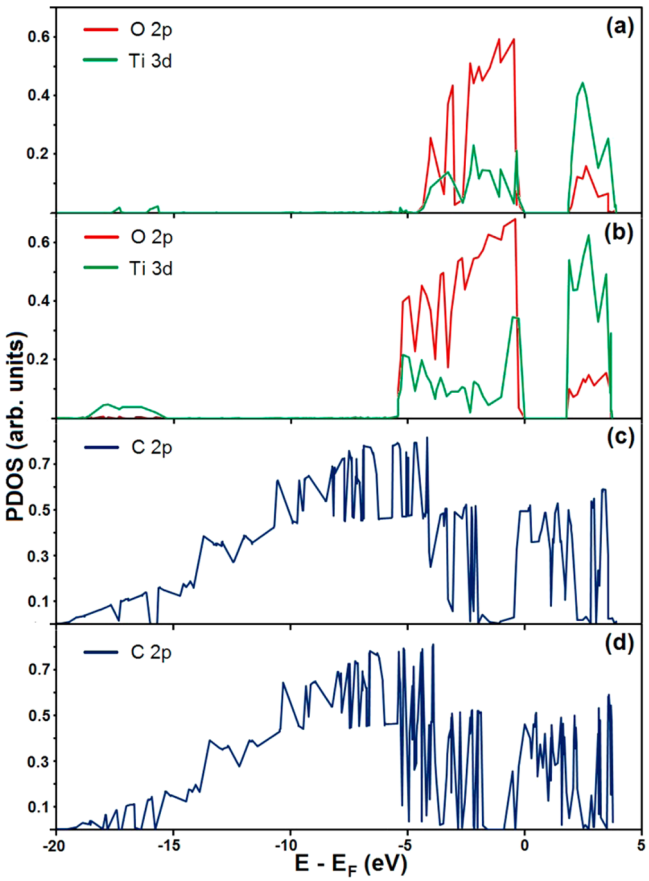

Figure 9. Partial density of states (PDOS) of (a) Ti 3d and O 2p bands of rutile (Ti_2O_4) adsorbed at graphene, (b) Ti 3d and O 2p bands of anatase (Ti_4O_8) adsorbed at graphene, (c) C 2p band of graphene substrate with rutile (Ti_2O_4) adsorbed, and (d) C 2p band of graphene substrate with anatase (Ti_4O_8) adsorbed. The Fermi level is referenced at 0 eV.

and 9b for oxygen and titanium, respectively. PDOS for C 2p bands are displayed in Figure 9c and 9d for graphene with adsorbed rutile (Ti_2O_4) and anatase (Ti_4O_8) nanoclusters, respectively. To facilitate an understanding of how the O 2p, Ti 3d, and C 2p states are modified upon nanostructure adsorption, the C 2p band of graphene was isolated from that of TiO_2 after adsorption of nanostructural TiO_2 for rutile (Ti_2O_4) and anatase (Ti_4O_8).

For the titania nanostructures, the PDOS of O and Ti atoms display clear semiconducting properties for both rutile (Ti_2O_4)

dx.doi.org/10.1021/jp403835m | J. Phys. Chem. C XXXX, XXX, XXX−XXX

and anatase (Ti_4O_8), respectively. Their valence and conduction bands are spaced around the Fermi level (E_F) referenced at 0 eV. The valence band is dominated by O 2p orbitals with a small contribution from the Ti 3d orbitals. Ti 3d dominates the conduction band with a small contribution from O 2p. The intrinsic band gaps of TiO_2 nanostructures have no changes, implying that the electron transition from the O 2p at the valence band and the Ti 3d at the conduction band is not the dominant process in the interactions between TiO_2 nanoclusters and graphene. The lower theoretical value of band gaps with respect to experimental data is caused by a shortage in the DFT estimation of band gaps due mostly to the self-correlation error of electrons and to the difference between small clusters and bulk matter.[43,44] Similarly, band gap oscillations have also been predicted for semiconducting narrow graphene ribbons as a function of their width.[45]

By comparing Figures 9c and 9d, it is immediately apparent that the C 2p band of graphene with rutile (Ti_2O_4) adsorbed is quantitatively similar to that of the C 2p band of graphene with anatase (Ti_4O_8) adsorbed. C 2p PDOS of graphene is also similar to that of the pure nondecorated graphene sheet. C 2p of graphene with metal oxide adsorption have no upward or backward movement of their Fermi levels as the titania adsorbates are nonmetallic and nonionic species. Some additional peaks below and above the Fermi level of graphene can be seen on the C 2p band of graphene with anatase adsorbed compared to the C 2p band of graphene in which rutile is adsorbed. We assume these peaks to be characteristic of structural defects of graphene substrate at the adsorption region.

Previously reported theoretical studies showed that well-known defects associated with the C atom dislocation or displacement are caused by a 5− defect in graphene[46] or epoxy bonds[47] (oxygen atom adsorbed on bridge sites of graphene). This defect causes the presence of multiple additional peaks around the Fermi level of PDOS C 2p of graphene. These peaks indicate that the electronic delocalization on graphene is weakened. The multiplication of peaks is also due to a propagation of C atom displacements around the 6−(6+Ti) defect inside of a large graphene supercell (100 atoms).

Within the qualitative electronic information provided here, it would appear that there is no clear positive correlation between the strength of the binding energy to the substrate and the qualitative extent of charge transfer determined by PDOS. This is due to the fact that noncovalent bonds were created by the physical adsorption process as the adsorbed nanostructural titania species are nonionic and the graphene susbstrate has no defects. To further analyze the difference between graphene C 2p with both rutile and anatase adsorption, we examine the C−C bond deformation of the graphene supercell. Figure 10 shows the effect of the adsorption distance of TiO_2 nanostructural species on the C−C bond deformation of the graphene supercell aound the adsorption region. First, this curve confirmed that anatase (Ti_4O_8) binds closer than rutile (Ti_2O_4) to the graphene substrate on all physical adsorption sites. However, C−C bonding of graphene is affected by nanostructural anatase significantly more than by rutile. The proximity of adsorption of anatase on graphene is an important factor in the level of local deformation of the graphene supercell where the adsorption occurs. The adsorption of rutile plays a lesser role in the C−C bond deformation of graphene, but the same general pattern is shown by both curves. This local C−C bond deformation of graphene explains qualitatively the higher

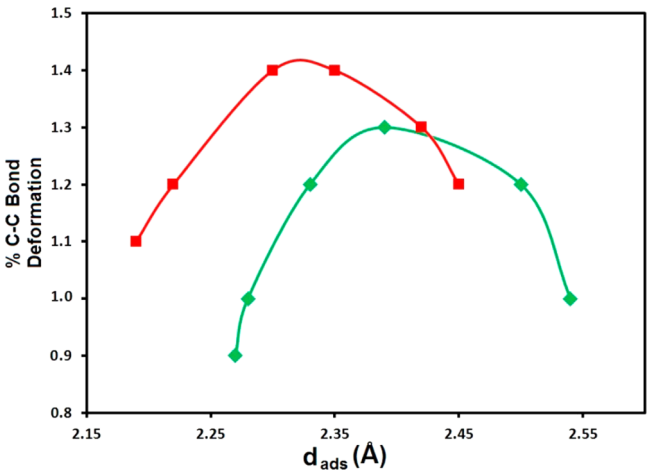

Figure 10. Percentage of C−C bond deformation of a graphene ring with a TiO_2 nanostructure adsorbed with respect to the C−C bond of an unoccupied graphene ring. The red curve shows the effect of an adsorbed anatase (Ti_4O_8) nanostructure on the C−C bond of graphene with respect to the distance of adsorption. The green curve shows the effect of an adsorbed rutile (Ti_2O_4) nanostructure on the C−C bond of graphene with respect to the distance of adsorption.

instability of the C 2p PDOS around the Fermi level where the 6−(6+Ti) defect occurs. As a result of tighter adsorption and a higher C−C bond deformation of graphene substrate, anatase (Ti_4O_8) while adsorbed on all physical adsorption sites is less favorable than rutile (Ti_2O_4). However anatase and rutile showed similar binding energies and distances on all chemical adsorption sites of functionalized GNRs.

4. CONCLUSION

We have studied the adsorption of molecular and structural TiO_2 adsorbates on pure graphene and functionalized graphene nanoribbons (i.e., −COOH, −OH, and −O−) by density functional theory (DFT). The results show that binding energies to graphene for structural TiO_2 nanocompounds such as rutile (Ti_2O_4) and anatase (Ti_4O_8) are higher than those from for simple TiO_2 molecule. TiO_2 nanostructures showed higher physical adsorption on clean graphene sheets and also on all of the chemical adsorption sites of a functionalized graphene nanoribbons. We concentrated our investigation on both the metal−carbon (Ti−C) and metal−oxygen (Ti−O) interactions with potential 2-dimensional rotation of the adsorbates that leads to new sites, termed "rotated".[26] The binding energy values between the TiO_2 adsorbates and graphene on "top" sites were found to be more favorable than those on the rotated top sites. The binding energy values of the TiO_2 adsorbates and graphene on the so-called "bridge" sites were less favorable than those on the rotated bridge sites. The normal and rotated hollow sites provided the highest physisorption values compared to any of the examined physical adsorption sites. The carboxylate adsorption sites showed the highest binding energy of all sites of functionalized graphene nanoribbons compared to epoxy and graphene-ol.

Rutile (Ti_2O_4) was found to have a better substrate−adsorbate charge transfer because of less local C−C bond deformation of the graphene substrate which led to a higher binding energy with respect to anatase. However, anatase (Ti_4O_8) was found to bind closer to graphene sheets than rutile on all physical adsorption sites. Finally, adsorbed TiO_2

dx.doi.org/10.1021/jp403835m | J. Phys. Chem. C XXXX, XXX, XXX−XXX

molecules showed the lowest binding energy and the longest distances of adsorption on all sites of graphene and functionalized graphene nanoribbons. These results show the utility of density functional theory for examining graphene–TiO_2 interactions for understanding the growth mechanisms for future experimental investigations with this promising system. The effect of defects in graphene on the strength of the binding energy and the electronic structure of substrate–adsorbate systems were demonstrated theoretically to be of importance, and extension of our work for experimentally examining defects in pure and functionalized graphene–titania systems is ongoing.[48−50]

■ ASSOCIATED CONTENT

Supporting Information

VASP Input Format files for the two investigated functionalized graphene nanoribbons (Armchair and Zigzag). This material is available free of charge via the Internet at http://pubs.acs.org.

■ AUTHOR INFORMATION

Corresponding Author

*E-mail: pcharpentier@eng.uwo.ca.

Notes

The authors declare no competing financial interest.

■ ACKNOWLEDGMENTS

The authors acknowledge the Natural Sciences and Engineering Research Council of Canada (NSERC Strategic) for financial support. The DFT calculations presented in this work were performed at the Surface Science Centre of the University of Liverpool, which is acknowledged for providing access to the VASP simulation package.

■ REFERENCES

(1) Bai, S.; Shen, X. P. Graphene-inorganic nanocomposites. *RSC Adv.* **2012**, *2*, 64−98.

(2) Huang, Y.; Liang, J. J.; Chen, Y. S. An Overview of the Applications of Graphene-Based Materials in Supercapacitors. *Small* **2012**, *8*, 1805−1834.

(3) Shao, Y. Y.; Wang, J.; Wu, H.; Liu, J.; Aksay, I. A.; Lin, Y. H. Graphene Based Electrochemical Sensors and Biosensors: A Review. *Electroanalysis* **2010**, *22*, 1027−1036.

(4) Pumera, M. Graphene-based nanomaterials for energy storage. *Energy Environ. Sci.* **2011**, *4*, 668−674.

(5) Geim, A. K.; Novoselov, K. S. The rise of graphene. *Nat. Mater.* **2007**, *6*, 183−191.

(6) Worsley, M. A.; Kucheyev, S. O.; Mason, H. E.; Merrill, M. D.; Mayer, B. P.; Lewicki, J.; Valdez, C. A.; Suss, M. E.; Stadermann, M.; Pauzauskie, P. J.; Satcher, J. H.; Biener, J.; Baumann, T. F. Mechanically robust 3D graphene macroassembly with high surface area. *Chem. Commun. (Cambridge, U.K.)* **2012**, *48*, 8428−8430.

(7) Castro Neto, A. H.; Guinea, F.; Peres, N. M. R.; Novoselov, K. S.; Geim, A. K. The electronic properties of graphene. *Rev. Mod. Phys.* **2009**, *81*, 109−162.

(8) Barone, V.; Hod, O.; Scuseria, G. E. Electronic structure and stability of semiconducting graphene nanoribbons. *Nano Lett.* **2006**, *6*, 2748−2754.

(9) Ramasubramaniam, A. Electronic structure of oxygen-terminated zigzag graphene nanoribbons: A hybrid density functional theory study. *Phys. Rev. B: Condens. Matter Mater. Phys.* **2010**, *81*, 245413-1−245413-6.

(10) Shenoy, V. B.; Reddy, C. D.; Ramasubramaniam, A.; Zhang, Y. W. Edge-Stress-Induced Warping of Graphene Sheets and Nanoribbons. *Phys. Rev. Lett.* **2008**, *101*, 245501-1−245501-4.

(11) Son, Y. W.; Cohen, M. L.; Louie, S. G. Energy gaps in graphene nanoribbons. *Phys. Rev. Lett.* **2006**, *97*, 216803-1−216803-4.

(12) Nakada, K.; Fujita, M.; Dresselhaus, G.; Dresselhaus, M. S. Edge state in graphene ribbons: Nanometer size effect and edge shape dependence. *Phys. Rev. B: Condens. Matter Mater. Phys.* **1996**, *54*, 17954−17961.

(13) Pelaez, M.; Nolan, N. T.; Pillai, S. C.; Seery, M. K.; Falaras, P.; Kontos, A. G.; Dunlop, P. S. M.; Hamilton, J. W. J.; Byrne, J. A.; O'Shea, K.; Entezari, M. H.; Dionysiou, D. D. A review on the visible light active titanium dioxide photocatalysts for environmental applications. *Appl. Catal., B* **2012**, *125*, 331−349.

(14) Varghese, O. K.; Paulose, M.; Grimes, C. A. Long vertically aligned titania nanotubes on transparent conducting oxide for highly efficient solar cells. *Nat. Nanotechnol.* **2009**, *4*, 592−597.

(15) Vivero-Escoto, J. L.; Chiang, Y. D.; Wu, K. C.-W.; Yamauchi, Y. Recent progress in mesoporous titania materials: Adjusting morphology for innovative applications. *Sci. Technol. Adv. Mat.* **2012**, *13*.

(16) Landmann, M.; Rauls, E.; Schmidt, W. G. The electronic structure and optical response of rutile, anatase and brookite TiO_2. *J. Phys.: Condens. Matter* **2012**, *24*.

(17) Amtout, A.; Leonelli, R. Optical Properties of Rutile near Its Fundamental Band Gap. *Phys. Rev. B: Condens. Matter Mater. Phys.* **1995**, *51*, 6842−6851.

(18) Tang, H.; Levy, F.; Berger, H.; Schmid, P. E. Urbach Tail of Anatase Tio_2. *Phys. Rev. B: Condens. Matter Mater. Phys.* **1995**, *52*, 7771−7774.

(19) Luo, Q. P.; Yu, X. Y.; Lei, B. X.; Chen, H. Y.; Kuang, D. B.; Su, C. Y. Reduced Graphene Oxide-Hierarchical ZnO Hollow Sphere Composites with Enhanced Photocurrent and Photocatalytic Activity. *J. Phys. Chem. C* **2012**, *116*, 8111−8117.

(20) Rana, F. Electron-hole generation and recombination rates for Coulomb scattering in graphene. *Phys. Rev. B: Condens. Matter Mater. Phys.* **2007**, *76*.

(21) Nguyen-Phan, T. D.; Pham, V. H.; Shin, E. W.; Pham, H. D.; Kim, S.; Chung, J. S.; Kim, E. J.; Hur, S. H. The role of graphene oxide content on the adsorption-enhanced photocatalysis of titanium dioxide/graphene oxide composites. *Chem. Eng. J. (Amsterdam, Neth.)* **2011**, *170*, 226−232.

(22) Sui, R. H.; Charpentier, P. Synthesis of Metal Oxide Nanostructures by Direct Sol–Gel Chemistry in Supercritical Fluids. *Chem. Rev.* **2012**, *112*, 3057−3082.

(23) Farhangi, N.; Medina-Gonzalez, Y.; Chowdhury, R. R.; Charpentier, P. A. Growing TiO_2 nanowires on the surface of graphene sheets in supercritical CO_2: Characterization and photoefficiency. *Nanotechnology* **2012**, *23*.

(24) Lucky, R. A.; Sui, R.; Lo, J. M. H.; Charpentier, P. A. Effect of Solvent on the Crystal Growth of One-Dimensional ZrO_2–TiO_2 Nanostructures. *Cryst. Growth Des.* **2010**, *10*, 1598−1604.

(25) Ruohong, Sui; Lo, J. M. H.; Charpentier, P. A. Infrared and Computational Studies on Interactions of Carbon Dioxide and Titania Nanoparticles with Acetate Groups. *J. Phys. Chem. C* **2009**, *113*, 21022−21028.

(26) Rojas, M. I.; Leiva, E. P. M. Density functional theory study of a graphene sheet modified with titanium in contact with different adsorbates. *Phys. Rev. B: Condens. Matter Mater. Phys.* **2007**, *76*, 21022−21028.

(27) Perdew, J. P.; Chevary, J. A.; Vosko, S. H.; Jackson, K. A.; Pederson, M. R.; Singh, D. J.; Fiolhais, C. Atoms, Molecules, Solids, and Surfaces: Applications of the Generalized Gradient Approximation for Exchange and Correlation. *Phys. Rev. B: Condens. Matter Mater. Phys.* **1992**, *46*, 6671−6687.

(28) Kresse, G.; Furthmuller, J. Efficiency of ab-initio total energy calculations for metals and semiconductors using a plane-wave basis set. *Comput. Mater. Sci.* **1996**, *6*, 15−50.

(29) Kresse, G.; Furthmuller, J. Efficient iterative schemes for ab initio total-energy calculations using a plane-wave basis set. *Phys. Rev. B: Condens. Matter Mater. Phys.* **1996**, *54*, 11169−11186.

(30) Blochl, P. E. Projector Augmented-Wave Method. *Phys. Rev. B: Condens. Matter Mater. Phys.* **1994**, *50*, 17953−17979.

(31) Kresse, G.; Joubert, D. From ultrasoft pseudopotentials to the projector augmented-wave method. *Phys. Rev. B: Condens. Matter Mater. Phys.* **1999**, *59*, 1758−1775.
(32) Monkhorst, H. J.; Pack, J. D. Special Points for Brillouin-Zone Integrations. *Phys. Rev. B: Solid State* **1976**, *13*, 5188−5192.
(33) Konkena, B.; Vasudevan, S. Understanding Aqueous Dispersibility of Graphene Oxide and Reduced Graphene Oxide through pK(a) Measurements. *J. Phys. Chem. Lett.* **2012**, *3*, 867−872.
(34) Evarestov, R. A.; Bandura, A. B.; Losev, M. V. Symmetry and stability of nanotubes based on titanium dioxide. *Russ. J. Gen. Chem.* **2010**, *80*, 1152−1167.
(35) Labat, F.; Baranek, P.; Adamo, C. Structural and electronic properties of selected rutile and anatase TiO_2 surfaces: An ab initio investigation. *J. Chem. Theory Comput.* **2008**, *4*, 341−352.
(36) Chretien, S.; Metiu, H. Electronic Structure of Partially Reduced Rutile TiO_2(110) Surface: Where Are the Unpaired Electrons Located? *J. Phys. Chem. C* **2011**, *115*, 4696−4705.
(37) Hmiel, A.; Xue, Y. Q. Quantum confinement and surface relaxation effects in rutile TiO_2 nanowires. *Phys. Rev. B: Condens. Matter Mater. Phys.* **2012**, 85.
(38) Tosoni, S.; Lamiel-Garcia, O.; Hevia, D. F.; Dona, J. M.; Illas, F. Electronic Structure of F-Doped Bulk Rutile, Anatase, and Brookite Polymorphs of TiO_2. *J. Phys. Chem. C* **2012**, *116*, 12738−12746.
(39) Li, X. L.; Qi, W.; Mei, D. H.; Sushko, M. L.; Aksay, I.; Liu, J. Functionalized Graphene Sheets as Molecular Templates for Controlled Nucleation and Self-Assembly of Metal Oxide-Graphene Nanocomposites. *Adv. Mater.* **2012**, *24*, 5136−5141.
(40) Savara, A. Standard States for Adsorption on Solid Surfaces: 2D Gases, Surface Liquids, and Langmuir Adsorbates. *J. Phys. Chem. C* **2013**, *117*, 15710−15715.
(41) Liu, L.; Shen, Z. X. Bandgap engineering of graphene: A density functional theory study. *Appl. Phys. Lett.* **2009**, 95.
(42) Mo, S. D.; Ching, W. Y. Electronic and Optical-Properties of 3 Phases of Titanium-Dioxide: Rutile, Anatase, and Brookite. *Phys. Rev. B: Condens. Matter Mater. Phys.* **1995**, *51*, 13023−13032.
(43) Mori-Sánchez, P.; Cohen, A. J.; Yang, W. T. Localization and delocalization errors in density functional theory and implications for band-gap prediction. *Phys. Rev. Lett.* **2008**, *100*, 146401-1−146401-4.
(44) Sham, L. J.; Schluter, M. Density-Functional Theory of the Energy-Gap. *Phys. Rev. Lett.* **1983**, *51*, 1888−1891.
(45) Ezawa, M. Peculiar width dependence of the electronic properties of carbon nanoribbons. *Phys. Rev. B: Condens. Matter Mater. Phys.* **2006**, *73*, 045432-1−045432-8.
(46) Charlier, J. C.; Ebbesen, T. W.; Lambin, P. Structural and electronic properties of pentagon-heptagon pair defects in carbon nanotubes. *Phys. Rev. B: Condens. Matter Mater. Phys.* **1996**, *53*, 11108−11113.
(47) Geng, W.; Liu, H. X.; Yao, X. J. Enhanced photocatalytic properties of titania-graphene nanocomposites: A density functional theory study. *Phys. Chem. Chem. Phys.* **2013**, *15*, 6025−6033.
(48) Banhart, F.; Kotakoski, J.; Krasheninnikov, A. V. Structural Defects in Graphene. *ACS Nano* **2011**, *5*, 26−41.
(49) Cockayne, E. Graphing and grafting graphene: Classifying finite topological defects. *Phys. Rev. B: Condens. Matter Mater. Phys.* **2012**, *85*, 125409-1−125409-6.
(50) Lherbier, A.; Dubois, S. M. M.; Declerck, X.; Niquet, Y. M.; Roche, S.; Charlier, J. C. Transport properties of graphene containing structural defects. *Phys. Rev. B: Condens. Matter Mater. Phys.* **2012**, *86*, 075402-1−075402-18.